Topological Defect Chains on Curved Surface

Stable Lattice Theory of Curved Surface Formation and Analyses of Simulations with Dimer Modelling

Chen Yuan* and Chen Qi†
Physics Department, Fudan University
(Fudan University, Shanghai)

The study of the ordered structure of soft matter systems and their mechanical response constitutes a fundamental class of scientific problems in the study of soft matter physics. When spatial constraints are imposed on a soft matter system, the system can exhibit a rich and unique ordered structure. Among them, the concepts of geometric frustration and topological defects have greatly expanded the understanding of matter ordering and orderliness. This thesis will be devoted to the study of the geometric structure and mechanical response of soft matter systems from a geometric perspective. Through two-dimensional modelling of surfaces of specific geometrical shapes and computer simulations to show the dislocation flow and geometrical defect chains on the surface of the soft matter, where we introduce dimer model to explain it, the influence of the long-range force factor on the bonding ratio is quantitatively analysed, which to some extent reflects the process of the phase transition from the gas phase to the liquid phase,and analyze the conditions for the formation of the glassy phase.

I. INTRODUCTION

Topological defects have played a crucial role in understanding the order, rigidity and melting of crystals and other phases of matter in two-dimensional flat space[1]. It may make phase transitions more complicated or lead to new phase transitions and physical phenomenons in some cases.

A. Topological defect resulting in pentagons and heptagons on a surface with curvature

To analyze the impact of geometric constraints and topological defects on crystals on a two-dimensional curved plane, we must first start with some topological concepts. The geometric Euler's theorem tells us:

$$V - E + F = 2 \tag{1}$$

where V represents the number of vertices, E represents the number of edges, and F represents the number of faces. Then we use it to discuss tessellation of the plane and the sphere. We know that regular hexagons can cover an entire plane without any gaps, forming a tight and symmetric structure. However, according to Euler's theorem and the topological properties of a sphere, it is impossible to completely cover a sphere with regular hexagons without defects. To cover a sphere, some other pentagons must be introduced. For instance, a soccer ball is covered with 20 regular hexagons and 12 regular pentagons. In fact, the Gauss-Bonnet theorem tells us that the total Gaussian curvature of a closed surface is related to its Euler characteristic:

$$\int_S K dA = 2\pi\chi(S) \tag{2}$$

where K is the Gaussian curvature of the surface. dA is the area element on the surface. $\chi(S)$ is the Euler characteristic of the surface.For a sphere (with an Euler characteristic of 2), the total Gaussian curvature must be 4π radians. Pentagons have positive curvature, hexagons have zero curvature, and heptagons have negative curvature. Thus, either on a sphere or on any plane with curvature, we need to use Pentagons and heptagons on the curved planes to balance the curvatures.

B. Topological defect's effects in KTHNY

Then we introduce the effects of curvature and topological defects into the KTHNY theory (Kosterlitz-Thouless-Halperin-Nelson-Young theory). The KTHNY theory describes the phase transition processes of two-dimensional crystals at different temperatures. The core of this theory is to discuss the phase transition behavior by analyzing defects such as dislocations and disclinations. This theory predicts the unbinding of topological defects to break the symmetry in two steps at two distinct temperatures: dissociation of dislocation pairs first melts the crystal into a still orientational ordered (hexatic) phase and, in the second step, dissociation of free dislocations causes the system to go isotropic fluid.[2]

A dislocation in a two-dimensional crystal is a defect that arises from the insertion of half lattice lines into the otherwise perfect lattice. Due to this lines a single dislocation cannot be made to disappear by any continuous

* These authors contributed equally to this work.; 22307110275@m.fudan.edu.cn
† These authors contributed equally to this work.; 22307110307@m.fudan.edu.cn

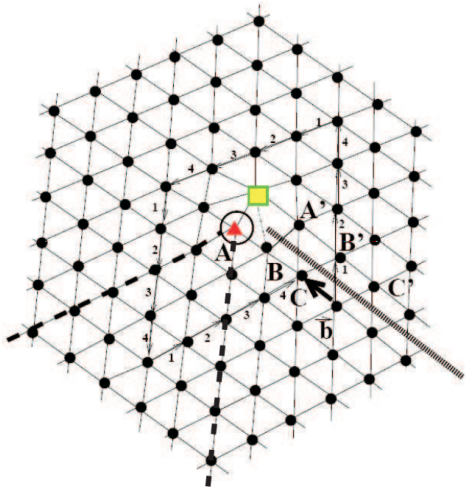

FIG. 1: **Dislocation in a triangular lattice with the thick dashed lines representing the inserted half lattice lines.** It can also be viewed as a special kind of defect pair, a 5-fold site being next neighbor to a seven-fold coordinated lattice site.The picture is from[2]

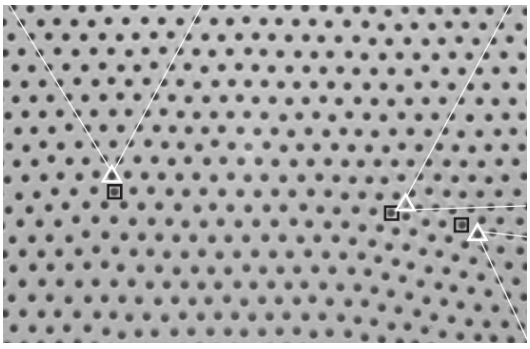

FIG. 2: **Micrograph of a colloidal crystal showing three isolated dislocations.** The black squares mark the seven-fold coordinated colloids and the triangles mark the five-fold coordinated particles representing the end of the inserted half lattice lines (white solid lines).The picture is from[2]

transformation. This is why a dislocation is a topological defect. Fig.1 shows a dislocation in a triangular lattice with the thick dashed lines representing the inserted half lattice lines (two lines in case of a hexagonal crystal due to symmetry). From the sketch it is also evident how one can come back to the regular lattice: Cutting the crystal along the hatched bar, one has to relax the distorted lattice by shifting the whole lattice on one side of the cut by the vector such that eventually the sites A and A', B and B', and C and C' are becoming connected again.

The figure shows that the last site at the end of the inserted half line has only five rather than the usual six next neighbors. Next to this site, there is a seven-fold coordinated site. So, a dislocation can be viewed as special kind of defect pair, a 5-fold site being next neighbor to a seven-fold coordinated lattice site. The topological defects caused by a pentagon and a heptagon here cancel each other out. A photograph of a real two-dimensional crystal showing a dislocation is given in Fig.2

In a flat two-dimensional planehow is this sudden occurrence possible if formation of a dislocation requires insertion of half a lattice line? The answer to this question is that single dislocations will never spontaneously form, but that dislocations will first appear in form of dislocation pairs which then can dissociate into single dislocations. And such pairs can evolve from local lattice displacements or the curvature of the surface and topological defects.

If sufficient thermal energy is provided, the dislocation pair can be excited to a higher bound state in which the pair distance is larger. Eventually this pair can completely dissociate into two dislocations. In this way two single dislocations are generated without there being the need to insert half lines.

But considering a curved plane, the pentagons and heptagons brought about by inherent topological defects will derectly result in such dislocations, which are not necessarily produced in pairs, and thereby affecting the KTNHY process.

The decay of order is not yet completed: the next step that may occur if enough thermal energy is available, is a dissociation of a single dislocation into an isolated five-fold coordinated site and another seven-fold coordinated site. These defects are disclinations. They form another class of topological defects in 2D solids. Disclinations destroys the residual orientational order. The system has entered into the isotropic fluid phase in which we have an exponential decay of both orientational and translational order parameter.[2]

In summary, the first defect type destroys the translational order and transforms the crystal into what is known as the 'hexatic phase', while occurrence of the second type of defect results in the destruction of the orientational order, leading to a phase transition into the fluid phase.Curvature and topological defects may have significant effects in KTNHY.

Firstly, the pentagons and heptagons brought about by Gaussian curvature and inherent topological defects will result in additional dislocations, thereby affecting the KTNHY process.

Secondly, they may influence the stability, mobility, interactions, and dissociation of dislocations. On a flat plane, dislocations can move freely. However, on a spherical surface, the curvature imposes geometric constraints on their movement, affecting their path and potentially altering the energy barriers associated with their motion, making movement easier or harder in regions with different curvatures. Due to the curvature, dislocations may be more stable in certain areas of the surface compared to others and are more diffiicult to dissociate into disclinations (an isolated five-fold coordinated site and a seven-fold coordinated site).

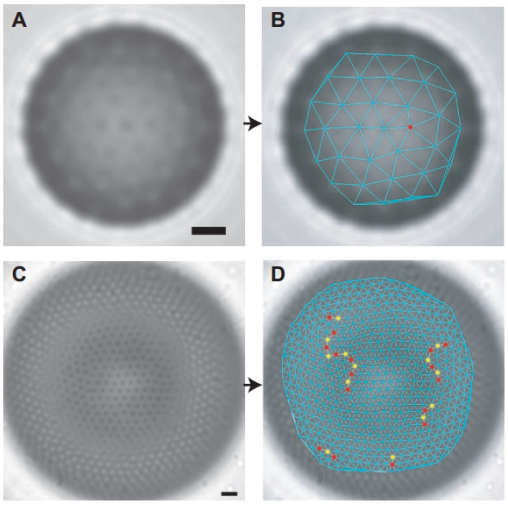

FIG. 3: **Light microscope images of two particle-coated droplets. (a)**$[R/a = 4.2]$ and **(c)**$[R/a = 14.3]$ and their associated defect structures **(b)** and **(d)**. The picture is from[3]

Additionally, on a flat plane, defects can move freely and distance themselves from each other, reducing interactions. But on a curved surface, particularly at high temperatures with a high defect concentration, interactions between defects may lead to more complex phase behavior.

C. Defect chains are formed under proper conditions

Experiments have found that pentagonal or heptagonal structures indeed appear on spherical surfaces(Fig.3). But as the ratio of the radius R to the average particle spacing a increases, except the pentagonal defects required by the spherical surface, many additional pairs of pentagons and heptagons are formed (with pentagon sites marked in red and heptagon sites in yellow in the figure). These additional defects form dislocation chains. One possible explanation is that as the radius increases, isolated disclinations become much more energetically costly. This elastic strain energy may be reduced by the formation of linear dislocation arrays, i.e., topological defect chains.[3]

To provide a more detailed image, we introduce a system of charged, hydrophobic microspheres adsorbed at oil–aqueous interfaces.[4] This system is particularly well characterized—its entire phase behaviour can be reduced to a one-dimensional phase diagram parameterized by a single, dimensionless interaction parameter,Γ, defined as the ratio of neighbour magnetic dipole and thermal energies:

$$\Gamma = \frac{(\pi\rho)^{3/2}}{k_B T} A \tag{3}$$

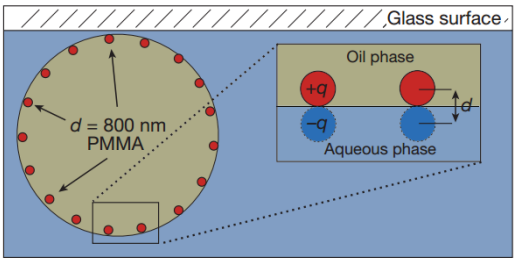

FIG. 4: **The particles are bound to the surface by electrostatic image charge forces,** and can uniformly decorate the surfaces of spheres, or other curved surfaces, without affecting the form of their interparticle forces. The picture is from[4]

where A quantifies the magnitude of the dipolar pair potential, $U(r) = A/r^3$ (where r is the separation between particles), ρ is the number density of particles.

Yet, unlike any system controlled by magnetic fields, these particles are bound to the surface by electrostatic image charge forces (Fig.4), and can uniformly decorate the surfaces of spheres, or other curved surfaces, without affecting the form of their interparticle forces.

The topology of the sphere fundamentally changes the KTHNY picture of ordering by elimination of defects, since at least twelve 5-coordinated disclinations (particles with pentagonal Voronoi cells and positive topological charge) are required. Furthermore, it has been discovered that as the size of the system increases (at constant density) it becomes energetically favourable to decorate these 12 disclinations with dislocations (topologically neutral, 5–7 disclination pairs) organized into linear structures called 'scars' or topological defect chains. The total number of dislocations in the system—proportional to the length of the scars—also grows as R/a, where R is the radius of the sphere and a is the interparticle distance.

Since dislocations are mobile defects that destroy both crystallinity and rigidity, it is worth study whether crystallization of particles confined to the surface of a sphere is possible, and whether the proliferation of defects leads to liquid or glassy phases.

Confocal micrographs (top of Fig.5) show clear differences between droplets with high and low Γ values. First, Voronoi tessellations of these surfaces show that disclinations (particles with topological charge equal to 6 less their coordination number) are uniformly cover the liquid-like sample, but are much rarer in the more ordered sample and are clustered in scars (middle panel of Fig.5). A similar pattern is shown by the two-dimensional bond-orientational order parameter that measures the orientation and degree of hexagonal order around each particle:

$$\psi_6(r_i, t) = \frac{1}{N_i} \sum_{j=1}^{N_i} e^{i6\theta_{ij}(t)} \tag{4}$$

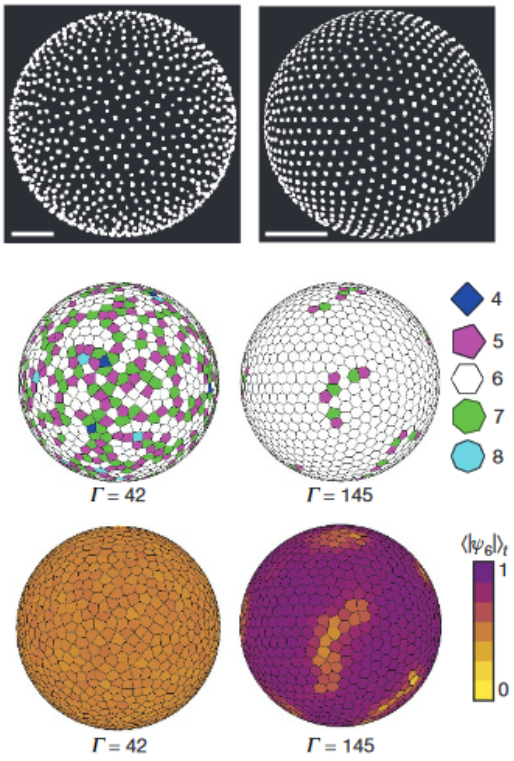

FIG. 5: **Confocal micrographs of droplets with high and lowΓ values.** Disclinations densely and uniformly cover the liquid-like sample, but are much rarer in the more ordered sample and are clustered in scars. The picture is from[4]

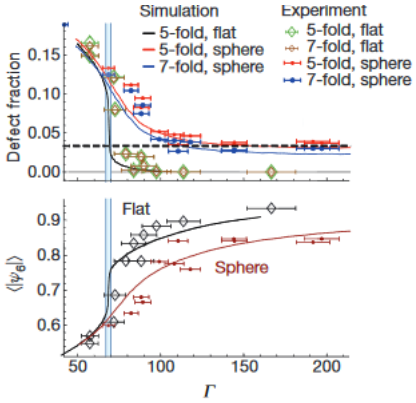

FIG. 6: **Measurements of defect fractions (top) and $\langle|\psi_6|\rangle$ (bottom) for spheres decorated with $N \approx 1,500$ particles and for similar particles on flat surfaces.** Symbols are experimental data points, with error bars defined in Supplementary Information section 2.2, while solid lines are simulation results.

Here, N_i is the coordination number of the ith particle, and $\theta_{ij}(t)$ is the angle between the line connecting particle i to its jth neighbour and an arbitrary reference axis. Like the distribution of topological defects (middle panel of Fig.5), the time-averaged $|\psi_6(r_b,t)|$, $\langle|\psi_6|\rangle_t$ is homogeneous over the entire sphere, as shown in the bottom panel of Fig. 1a. For the denser samples, $\langle|\psi_6|\rangle_t$ is spatially heterogeneous—the environment around most particles is locally hexagonal for the entire duration of observation, while a small number of particles, in or near the scars, have very low $\langle|\psi_6|\rangle_t$ values.

KTHNY theory postulates that the magnitude of this orientational order—as quantified, for example, by the $\psi_6(r_b,t)$ field averaged over space and time, $\langle|\psi_6|\rangle_t$—is intimately related to the distribution of topological defects. Indeed, in flat space the number of topological defects drops precipitously as the number of Γ values centred around $\Gamma \approx 70$, while $\langle|\psi_6|\rangle_t$ increases rapidly. By contrast, while the number of defects on spheres with $N = 1,500$ particles is accompanied by high $\langle|\psi_6|\rangle_t$, the crossover to high-Γ behaviour is broader (especially in the simulations) than what we observe in the flat layers; more clustering of topological defects reaches a plateau with a number much larger than that inferred by topology (Fig. 6). In the $\Gamma, N \to \infty$ limit, the number and clustering of defects has been predicted using continuum elasticity.[4]Flat surface packings eliminate nearly all defects and attain nearly perfect orientational order over a narrow range of Γ values ($\Gamma \approx 67 - 70$, shaded). For spherical packings, the improvement in local order and annihilation of defects with increasing Γ is dramatically hindered, with a finite concentration of defects expected even in the $\Gamma \to \infty$ limit; this is consistent with predictions based on continuum elasticity (dashed horizontal line).

Yet, although these globally averaged quantities reflect the increasing order of particles with increasing Γ, they do not reflect the clustering of defects that is evident in the micrographs. To understand this clustering better, $g_{55}(r)$ should be computed, which reflects the pair correlation between 5-coordinated defects, for experimental and simulated particle configurations over a wide range ofΓ. It is found that $g_{55}(r)$ is flat for $\Gamma < 70$, which consistents with a random distribution of defects. However, for $\Gamma > 70$, a peak is found in $g_{55}(r)$at short distances that grows and widens with increasing Γ—indicating the condensation of defects into clusters. (Fig.7)More interestingly, additional peaks in $g_{55}(r)$appear for values of r that correspond to the geodesic distances between the vertices of an icosahedron , making it possible to draw a football on the sphere such that most of the defects lie inside its pentagons (Fig.7). Nevertheless, this icosahedral ordering of defects develops gradually, and it is difficult to unambiguously identify isolated defect clusters until $\Gamma > 120$.

We consider $\Gamma \approx 120$. The strong coupling between lattice defects and particle mobility in crystalline solids suggests that the proliferation and spatial segregation of dislocations will also affect the dynamics of our system. To study this, we adopt a tool used to describe glasses, labeling particles that move more than a distance λ^* over

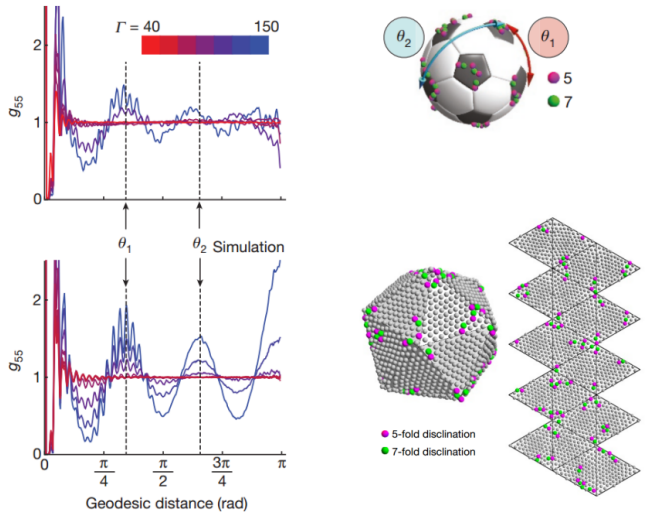

FIG. 7: **Topological defects in polyhedra.**Left is the graphs of $g_{55}(r)$ at different Γ. Upper right shows that it is possible to draw a football on the sphere such that most of the defects lie inside its pentagons. And lower right is an expansion diagram of an icosahedron with vertices distributed with defect chains. The picture is from[4]

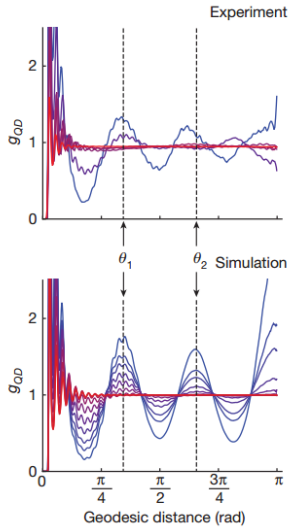

FIG. 8: **Pair cross-correlations of all defects and mobile particles for the same spheres.** It shows similar ordering to g_{55}, demonstrating the spatial coincidence of defects and mobility. The picture is from[4]

a time τ^* as 'mobile' ($Q = 1$) and those that do not as 'caged' ($Q = 0$) (Supplementary Information section 6). For large values of Γ, we observe clustering of mobile particles reminiscent of the clustering of topological defects. To investigate the connection between defects and mobility, we compute $g_{QD}(r)$, the pair correlation function between mobile particles ($Q = 1$) and disclinations (D, defined as particles with any coordination number other than six). We find that $g_{QD}(r)$ is almost identical to $g_{55}(r)$, confirming that particle mobility is strongly heterogeneous and becomes confined to the same icosahedrally coordinated 'seas' that contain the excess lattice defects.

In two dimensions, long-range correlations of orientational order, captured by $\psi_6\psi_6^* = \langle|\psi_6(r)\psi_6(0)^*|\rangle = g_6(r)$, are a clear sign of crystallinity; however, vector transport on the sphere changes angles and complicates the definition of a global reference coordinate system. Nevertheless, the icosahedral ordering of defects suggests that it may be possible to detect crystalline order by explicitly referencing this broken symmetry. We thus define an icosahedral 'net' by rotating an icosahedron so that its vertices are aligned with the positions of the defects.We quantify this order using the icosahedrally referenced orientational correlation function:

$$\psi_6\psi_6'^* = \langle\psi_6(r)\psi_6(0)'^*_{(}\cos^-1(r_i r_j)^2)\rangle) = r \qquad (5)$$

where $\psi_6'^*$ is the icosahedrally referenced value of the bond-orientational order parameter. We note that randomly oriented icosahedral nets, or nets based on polyhedra with different symmetries, will not produce such coherence.

The emergence of this new broken symmetry raises the question of whether the extreme retardation in the growth of $\langle|\psi_6|\rangle_t$ is a finite-size effect, or arises because the spherical geometry fundamentally changes the form of the freezing transition, perhaps requiring an additional order parameter to describe it. Consequently, to explore the $N \to \infty$ limit, we supplement simulations of spheres decorated with with $N = 1,500$ particles, with simulations with $N = 3,000, 6,000$ and $12,000$ particles, and evaluate two order parameters: the icosahedrally referenced two-dimensional bond-orientation of the particles Ψ_6'= $\frac{1}{N}\sum_i \psi_6'(r_i)$and the normalized, three-body, three-dimensional bond-orientation of the defects$\widetilde{W}_6$:

$$\widetilde{W}_6 = -\frac{\sqrt{4199}}{11}\sum_{m_1,m_2,m_3=-6}^{6}\begin{pmatrix}6 & 6 & 6\\ m_1 & m_2 & m_3\end{pmatrix}\frac{\rho_{6m_1}\rho_{6m_2}\rho_{6m_3}}{(\sum_m|\rho_{6m}|^2)^{3/2}} \qquad (6)$$

where the first quantity in the summand is the Wigner 3-j symbol and $\rho_{6m} = \sqrt{4\pi}\sum_i Y_{6m}(\theta_i,\phi_i)$($Y_{6m}$ are the sixth-order spherical harmonics, and (θ_i,ϕ_i) are the polar coordinates of the ith defect). This order parameter is particularly sensitive to the presence of icosahedral symmetry, and is normalized so that $\widetilde{W}_6 = 1$ for a perfect icosahedron.

Plots of these quantities show that increasing the system size increases the rate at which orientational and icosahedral order increase with increasing Γ. A polynomial extrapolation of $\langle|\Psi_6'|^2\rangle$in powers of $1/R \propto$

$1/\sqrt{N}$shows that, in the thermodynamic ($N \to \infty$) limit, $\langle|\Psi_6^{'}|^2\rangle$vanishes for $\Gamma < 67$, but remains finite for $\Gamma > 70$, coinciding with the two-dimensional liquid and crystal phase boundaries. Similarly,$\widetilde{W}_6 = 1$ is zero for lower Γ, and begins to increase roughly linearly——with a slope approximately proportional to N—above a critical threshold. We note that both of these order parameters $\langle|\Psi_6^{'}|^2\rangle$ and $\widetilde{W}_6 = 1$ exhibit transitions close to the Γ values of the liquid– hexatic and hexatic–solid transitions in flat space as $R \to \infty$.

We define an icosahedral 'net' by rotating an icosahedron so that its vertices are aligned with the positions of the defects. Projecting the particles onto the faces of the icosahedron and unfolding the structure onto a plane reveals the remarkable global orientational coherence of particle configurations with highΓ (Fig.7). It can be observed that defect chains accumulate at the vertices of the icosahedron. Upon unfolding the icosahedron, it is found that there are indeed 12 more 5-fold disclinations than 7-fold disclinations, which is consistent with Euler's theorem that requires a sphere to have 12 pentagonal topological defects.

The elucidation of order by the unravelling and flattening of an appropriate polyhedral net is also useful in any curved surfaces. Moreover, the segregation of defects to symmetric sites, and the concomitant mobility near these sites, are useful in studying structures alike.

II. TWO-DIMENSIONAL POTTS MODEL AND DIMER MODEL

A. potts model

Given that our subsequent simulation model is very similar to the Potts model, we need to briefly introduce the Potts model first. The Potts model was proposed by British physicist Renfrey B. Potts in 1952 to study phase transition phenomena in statistical mechanics. It has important applications in the fields of statistical mechanics and phase transition theory, materials science, image processing, and computer vision. It is a generalization of the Ising model, which can be regarded as a system of interacting spins that can be either parallel or antiparallel, whereas the Potts model is a system of spins confined in a plane, with each spin pointing to one of the q equally spaced directions specified by the angles[5]:

$$\Theta_n = \frac{2\pi n}{q}, n = 0, 1, ..., q-1 \tag{7}$$

In the most general form the nearest-neighbor interaction depends only on the relative angle between the two vectors. This is quite generally known as a system of$Z(q)$symmetry whose Hamiltonian reads:

$$\mathcal{H} = -\sum_{ij} J(\Theta_{ij}) \tag{8}$$

where the function $J(\Theta)$ is 2π periodic and Θ_{ij} is the angle between the two spins at neighboring sites i and j. The $Z(q)$ model plays an important role in the lattice gauge theories and has attracted a growing interest.

The model suggested by Domb (Potts, 1952) is to choose

$$J(\Theta) = -\epsilon_1 \cos\Theta \tag{9}$$

Using a Kramer-Wannier (1941) type analysis, Potts was able to determine the critical point of this model on the square lattice for $q = 2, 3, 4$. While unable to extend this finding to $q > 4$, Potts reported as a remark at the end of his paper (Potts, 1952) the critical point for all q of the following model:

$$J(\Theta_{ij}) = \epsilon_2 \delta_{Kr}(n_i, n_j) \tag{10}$$

In addition to the two-site interactions, there can also be multisite interactions as well as external fields. For a Potts model on a lattice G of N sites, the Hamiltonian $\mathcal{H}$generally takes the form:

$$\begin{aligned} -\beta\mathcal{H} =& L\sum_i \delta_{Kr}(\sigma_i, 0) + K\sum_{i,j} \delta_{Kr}(\sigma_i, \sigma_j) \\ &+ K_3 \sum_{i,j,k} \delta_{Kr}(\sigma_i, \sigma_j, \sigma_k) + \cdots \end{aligned} \tag{11}$$

where $\beta = 1/kT$, and $\sigma_i = 0, 1, ..., q|1$ specifies the spin states at the ith site and

$$\begin{aligned} \delta_{Kr}(\sigma_i, ..., \sigma_k) &= 1, if \sigma_i = ... = \sigma_k \\ &= 0, otherwise \end{aligned} \tag{12}$$

Here $K = \beta\epsilon_2, K_n, n \geq 3$, is the strength of the n-site interactions, and$L$ is an external field applied to the spin state 0. The partition function is:

$$Z_G(q; L; K; K_n) = \sum_{\sigma_i=0}^{q-1} \exp\left(-\beta\mathcal{H}\right) \tag{13}$$

The physical properties of the system are derived in the usual way by taking the thermodynamic limit. Relevant thermodynamic quantities include the per site "free energy":

$$f(q; L; K; K_n) = \lim_{N\to\infty} \frac{1}{N} \ln Z_G(q; L; K; K_n) \tag{14}$$

The critical exponents α, $\alpha\prime$, β, γ, $\gamma\prime$,δ,...can be defined in the usual fashion from the singular behavior of these thermodynamic quantities near the critical temperature T_c.

In the next section, we will study the surface :$z = \sin(x)\sin(y)$and perform computer simulations on it (detailed content is in the next section). Fig.7 shows the projection of this surface onto an equivalent plane, where the white areas indicate positive curvature and the black areas indicate negative curvature. The defect chains

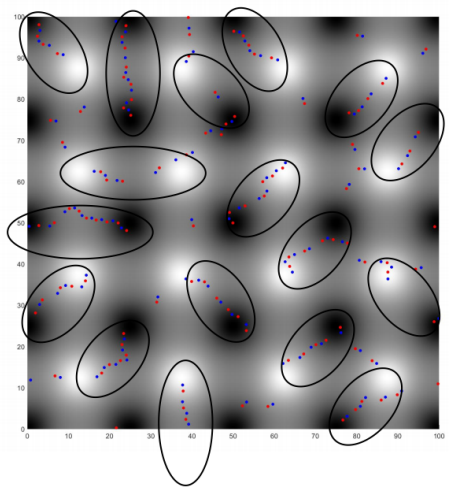

FIG. 9: The projection of the surface onto an equivalent plane and the characteristics of defect chains distributed on it.

distributed on the surface were obtained using pseudo-molecular dynamics, with red dots representing 5-fold disclinations and blue dots representing 7-fold disclinations. Based on the behavior of topological defect distribution on a sphere analyzed in the previous section, this distribution of defect chains is reasonable. Close observation reveals that the defect chains connect positive curvature (white) to positive curvature (white), negative curvature (black) to negative curvature (black), or positive curvature (white) to negative curvature (black).

A model similar to the Potts model can be constructed, as shown in Fig.8, where red and blue represent areas of positive and negative curvature. The arrows at the red or blue areas can take eight directions uniformly distributed around a circle. If the arrows of two points are exactly aligned, a bond is formed, or a chain is created. If we only consider the interaction energy between adjacent differently colored points and adjacent same-colored points, it can be expected that the bonding or chaining scenarios will differ depending on the values of ϵ_{ij} and ϵ_{ik} (Fig.8). We can use the methods similar to that used for the Potts model.

B. Dimer Model

In order to simplify the lattice model on a 3D surface, we most often convert the lattice to a 2D scatter lattice model. We are interested in the behaviour of the discontinuous phase transition of the lattice - to better describe this behaviour we introduce the dimer model.

The dimer model arose initially as an attempt to describe the adsorption of diatomic molecules on the surface of crystals, and has had success in describing the behavior of partially dissolved crystals in equilibrium. It has since been applied as a model for many other physical

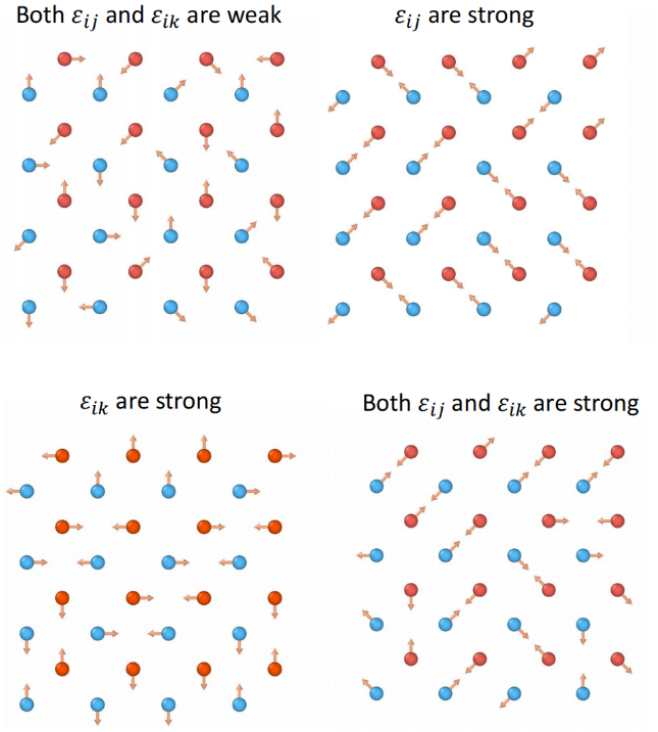

FIG. 10: Different bonding conditions with different values of ϵ_{ij} and ϵ_{ik}.

systems, and garnered much interest from the mathematical community, due in part to the tractibility afforded by a closed form expression for the partition function in certain cases. The model also exhibits conformal invariance in the classical setting, and can be understood in the context of $\mathbb{Z}_2$ gauge theory.

Quantum versions of the dimer model were proposed in studies of high temperature superconductors, specifically in the study of SU(2) singlet dominated phases in various spin models. Taking advantages of dimer model, we may develop a graph algorithm that generates a geometrically consistent dimer model with any fixed characteristic polygon, matching 5-7 edge lattice defect chains projected onto a plane.[6]

We consider a system which can be modeled as a graph $\mathbb{G}$. States of this system are defined as follows: given a graph $\mathbb{G}$, a perfect matching $\mathbb{M}$ of $\mathbb{G}$, also called a dimer conguration, is a subset of edges of G such that every vertex is incident to exactly one edge. Clearly, not all graphs satisfy matchings, and that is when we concentrate on certain structures.Fix some graph G, and consider any positive function on the edges of the graph $\nu : E \to \mathbb{R}$, called a weight function on G. The *energy* of a dimer configuration M will be defined as

$$\mathcal{E}(M) = -\sum_{e \in M} \log \nu(e), \tag{15}$$

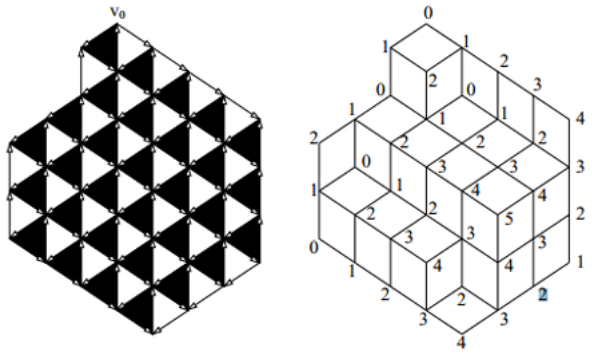

FIG. 11: **A triangular lattice, and a particular choice of height function.** Source: [13]

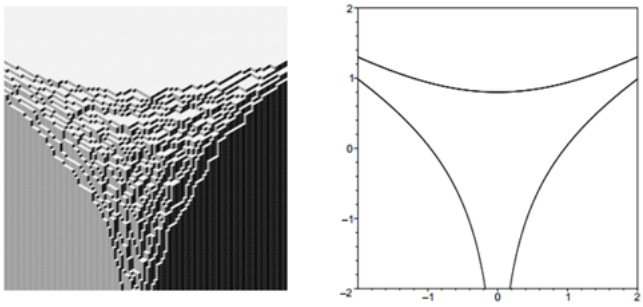

FIG. 12: **A height function arising from dimers on the honeycomb lattice.** One can imagine this as a 2D projection of the partially dissolved corner surface of a 3D crystal. On the right is a Ronkin function characterizing this height function. The picture is from[12]

and the *Boltzmann weight* of the configuration will be

$$\nu(M) = e^{-\mathcal{E}(M)} = \prod_{e \in M} \nu(e). \tag{16}$$

The Boltzmann weight divided by the partition function gives a Boltzmann measure on dimer configurations of $\mathbb{G}_{\ltimes}$. For a constant weight function $\nu(e) = 1$, the partition function simply counts the number of dimers. A key step is finding an explicit expression to compute the partition function.

Theorem: For a finite, bipartite, planar directed graph $\mathbb{G}_{\ltimes}$ with an admissible orientation of its edges, and a weight function ν, the partition function $Z(G)$ is given by the determinant of the Kastelyn matrix K associated with $\mathbb{G}_{\ltimes}$.Using this result, one can compute the probability of a particular set of edges in a dimer configuration according to the Boltzmann measure, providing insights into local statistics.

Here we discuss a method whereby dimer congurations can be associated with objects called height functions. These play a crucial role in finding closed form expressions for the graphs $\mathbb{G}_{\ltimes}$ mentioned in the previous section, and also provide alternative descriptions of dimer phenomena in general. An example is shown in Fig.11 Let G be a bipartite graph. A flow on G is a real valued function defined on all oriented edges of G, $\phi : E \to \mathbb{R}$. Note that we have not specified an orientation for G here yet; rather, E is the set of all possible oriented edges of G, so it contains two oppositely oriented copies of every edge of G. The divergence of a flow will be a real valued function on the vertices of G, $\mathrm{div}(\phi) : V \to \mathbb{R}$, which subtracts the total flow going into a vertex from that going out of it.[6]

A dimer configuration M on G can be used to define a flow as follows. Color the vertices of G white and black, and then choose ϕ to be 1 for every directed edge e such that $e \in M$ and e begins on a white vertex. Likewise, choose ϕ to be -1 for every directed edge e such that $e \in M$ and e begins on a black vertex. It is easily verified that the difference in flows $\phi_2 - \phi_1$ constructed in this way from two dimer configurations M_1, M_2, must have no divergence. Now consider any two faces f_0, f_1 in G, and an arbitrary path γ in the dual graph G^* from f_0 to f_1. The fact that $\phi_2 - \phi_1$ is divergence-free can be shown to imply that the flux of $\phi_2 - \phi_1$ across γ is independent of the choice of γ. This means this quantity is a function of the face f_1 only, once we choose a reference face f_0. If we further choose a fixed reference dimer configuration M_1, then we see that we have constructed one such function on the faces of G for every dimer configuration M_2.

This is the height function associated to M_2, and one can recast the theory of dimer models into a theory of appropriate height functions. This is one means by which dimer models can be used to understand the physics of partially dissolved crystals.[6] In the context of physics, the height function provides a way to visualize and analyze the dimer configurations. It can be interpreted as the surface height of a partially dissolved crystal where dimers represent bonds between atoms.

We should check that this is well-defined (i.e., it does not matter which edge we choose to cross when moving between regions). Let e_0 and e_1 be consecutive edges in the boundary between the regions B_1 and B_2 of R^2 ($M \subset M_0$). By the definition of a perfect matching, e_0 and e_1 cannot be part of the same perfect matching. Suppose, without loss of generality, that e_0 is in M_0 and e_1 is in M. If the crossing from B_1 to B_2 through e_0 has a black (resp. white) vertex on the right, then the crossing from B_1 to B_2 through e_1 has a black (resp. white) vertex on the left. Then the change in the height function is the same regardless of which edge is crossed. [7]

For example, in square lattice, dimer has exactly 4 perfect matchings, corresponding to the choice of a single edge of the dimer model. For the first two of these matchings, the associated perfect matchings of the universal cover are shown13. Fixing the reference matching to be the blue matching, we obtain their symmetric dif-

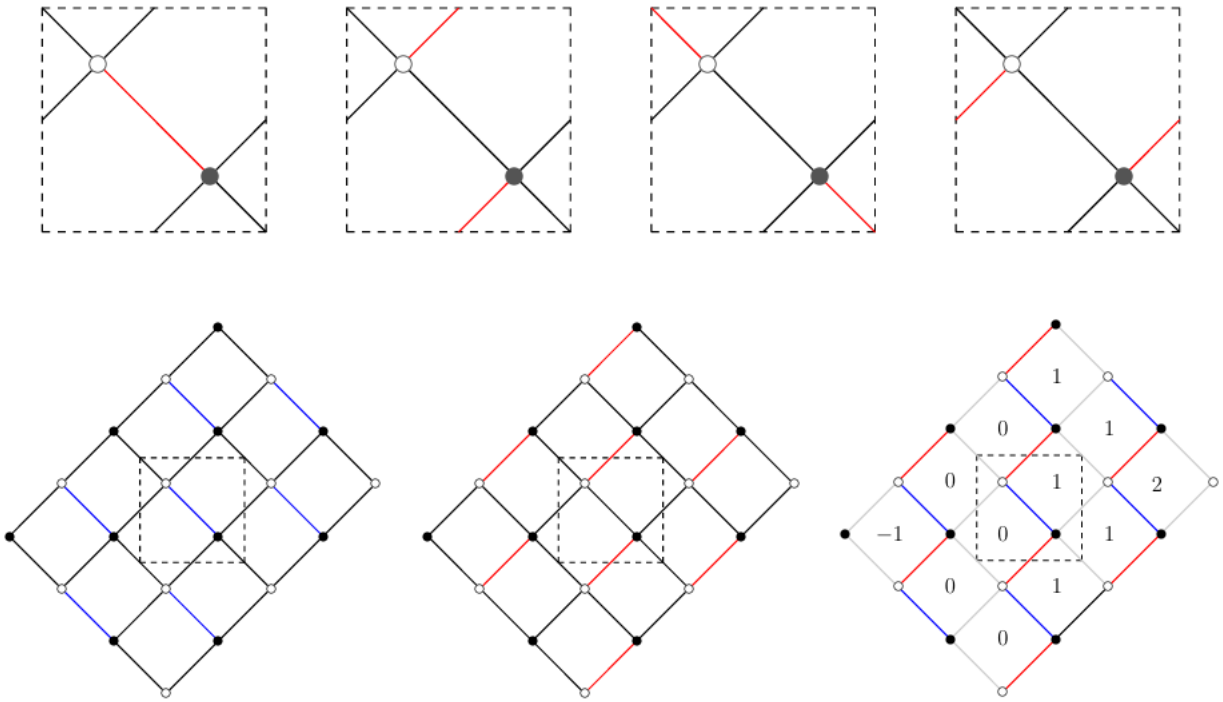

FIG. 13: **Schematic representation of the height function of a square dimer.** It can be seen that the choice of orientation does not have an effect on the energy.The figure is from[7].

ference and height function.

Applying this argument inductively, it does not matter at all which edge in the boundary of B_1 and B_2 we cross; we will always get the same change in the height function.

Meanwhile, we can also choose a preferred orientation for G_n when the graphs are bipartite. Then if we are given two weight functions ν_1, ν_2 on G, the functions are said to be gauge equivalent if they differ by the differential of a one-form:

$$\nu_1 = \nu_2 + df \quad \text{for some} \quad f \in (\Omega^0 \tag{17}$$

Here, Ω^0 is just the linear space of real functions on the vertices. More explicitly, this means:

$$\forall e = (wb) \in G_n, \nu 1(e) = \nu(e) + f(b) - f(w) \tag{18}$$

Given two gauge equivalent weight functions, the difference in energies $E_1(M) - E_2(M)$ for some dimer configuration M of G_n will be a constant. Since this energy difference will be the same for all dimer configurations, the two weight functions will actually induce the same Boltzmann distributions, and thus the same physics.

In physics, the phases of the classical dimer model can be characterized by studying the behavior of height functions.On a heuristic level, frozen phases are those in which there is some degree of determinism in height differences between different faces, gaseous phases are those in which height difference fluctuations have bounded variance, and liquid phases are those in which height differences grow universally as the logarithm of the distance between faces.

We introduce the convention that the points of a configuration shall be indicated in the following ("canonical") order:

$$P_1 < P_2; \quad P_3 < P_4; \quad \ldots; \quad P_{mn-1} < P_{mn}; \tag{19}$$

$$P_1 < P_3 < \ldots < P_{mn-1}. \tag{20}$$

By analogy to the determinantal approach to the Ising problem developed by Kac and Ward [8], we shall try to construct a mathematical form consisting of a series of terms each of which corresponds uniquely to one configuration and has the "weight" $z^{N_t} z'^{N'_t}$ of this configuration. The conditions (3) strongly suggest that this form should be a Pfaffian rather than a determinant. A Pfaffian is a number attributed to a triangular array of coefficients $a(k;k')$ $(k = 1, \ldots, N; k' = 1, \ldots, N; k < k'; N$ even) in the following way [9]:

$$\mathrm{Pf}\{a(k;k')\} = \sum_P \delta_P a(k_1;k_2)a(k_3;k_4)\ldots a(k_{N-1};k_N), \tag{21}$$

where the sum runs over those permutations $k_1, k_2, \ldots, k_N$ of the numbers $1, 2, \ldots, N$ which obey

$$k_1 < k_2; \quad \ldots; \quad k_{N-1} < k_N; \quad k_1 < k_3 < \ldots < k_{N-1}, \tag{22}$$

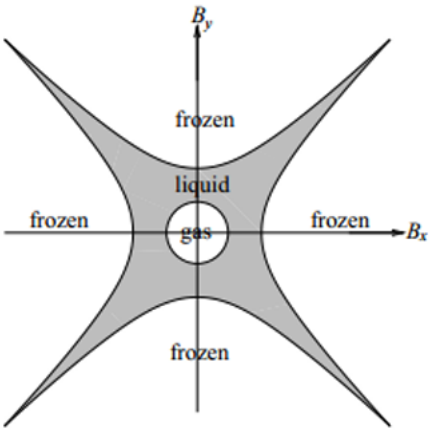

FIG. 14: This amoeba describes the phases of a particular dimer model in magnetic field coordinate space. This figure is from[13]

and where b_p is the parity of the permutation P, i.e. -1 or $+1$ according as P is an odd or an even permutation. Pfaffians have been introduced into physics by Caianello and Fubini and in lattice-combinatorial problems by Hurst and Green[10]. We shall now show that it is possible indeed to define a triangular array of elements $D(P;P')$ so that

$$Z_{mn}(z,z') = \mathrm{Pf}\{D(p;p')\}. \tag{23}$$

We begin by noting that if we define $D(P;P') = 0$ for all pairs of sites $(P;P')$ that are not connected by a bond, all terms in the Pfaffian that would not correspond to a dimer configuration will vanish. Next, we put the coefficients $D(P;P')$ corresponding to pairs of sites that are connected by a horizontal or a vertical bond equal, in absolute magnitude, to Z and z', respectively. In this way, we get all configurations represented by a term of the proper weight.[11]

One can associate a curve known as the spectral curve to any dimer model on a graph G, and these curves have very nice algebraic properties, being what are known as plane algebraic Harnack curves. Furthermore, they allow detailed information about phase diagrams to be extracted relatively simply. One such example of this is that the genus of the spectral curve associated to a dimer model is the number of distinct gaseous phases that arise in the model. This story is quite involved; just note that the classical dimer model has surprising ties to algebraic geometry, and there exists powerful machinery that has allowed for the phases of the classical models to be understood on a very deep level.

III. SURFACE TOPOLOGY DEFECT MODELLING

Based on the above discussion of the dimer model, when dealing with surface lattices in the presence of topological defect chains, we can consider the fixed edges graphs G_n in dimer flow. When we choose certain orientation, it will develop as height function, causing fluctuation in energies. At the same time, there is also a phase transition threshold for interactions if we only consider topological defect changes in the immediate and second immediate neighbourhood. Next we will perform computer simulations based on the dimer model for a specific lattice model in order to predict stable energy and phase transition point. Now we consider the more complex case on regular surfaces:

$$z = \sin(x)\sin(y) \tag{24}$$

We consider this as a dimer model, with corresponding new topological defects depending on the direction of flow. On this curved surface we generate a stable lattice. Referring to Fig. 15a, We can see that in the part of the Gaussian curvature with positive curvature (i.e., the peaks and valleys) there is a pentagonal phase, and in the part of the negative curvature (i.e., what we often call the "saddle surface" part) there is a heptagonal phase. We used different colours for the pentagonal, hexagonal and heptagonal lattices, and found that the pentagonal and heptagonal phases are often connected - this is determined by Euler's theorem, which we have described earlier. There is a seven-fold coordinated site. So, a dislocation can be viewed as special kind of defect pair, a 5-fold site being next neighbor to a seven-fold coordinated lattice site where the vector pointing along the bond connecting these two sites is almost perpendicular to the Burgers vector.[18]This is what we call a chain of topological defects. Note that the surface visualisation here uses a pseudo-molecular dynamics approach. There may be discrepancies with the experimental surface data.

For this system, interaction forces such as Coulomb forces still exist in the stable state of the lattice, causing particles to vibrate within the lattice, and particles in different topologically defective lattices bond with each other, which along with the vibrations, affects the macroscopic steady state energy. As we all know:

$$\mathcal{H} = \sum_{i=1}^{N}\left[\frac{1}{2m_i}\mathbf{p}_i^2 + \sum_{j=i+1}^{N} V_{ij} + \lambda_i g(\mathbf{x}_i)\right] \tag{25}$$

Constraint:

$$g(\mathbf{x}_i) = 0 \tag{26}$$

And we get:

$$\frac{d\mathbf{x}_i}{dt} = \frac{\partial \mathcal{H}}{\partial \mathbf{p}_i} = \frac{1}{m_i}\mathbf{p}_i \tag{27}$$

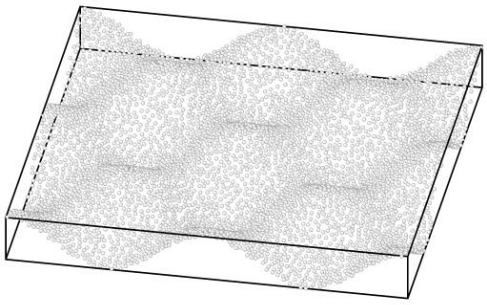

(a)

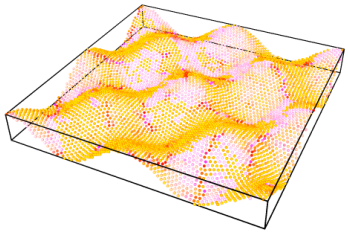

(b)

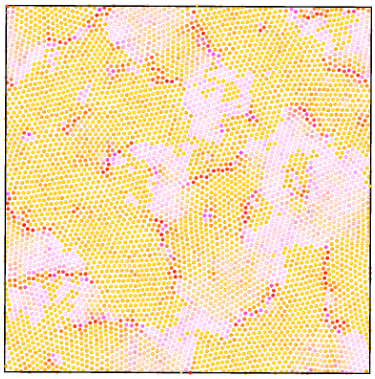

(c)

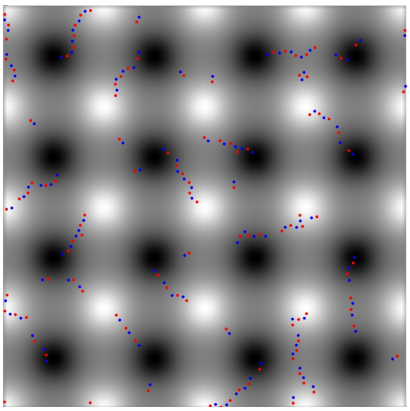

(d)

FIG. 15: **Surface visualisation diagram. (a)** particle visualisation for generating a stable lattice on a surface, **(b)** different topological defects are indicated using different colours, yellow: positive curvature region and no topological defects, pink: negative curvature region and no topological defects, orange: 5-fold disclination, red: 7-fold disclination, it can be observed that the 5-fold disclination is connected to the 7-fold disclination. **(c)** Top view of the planar topological defect visualisation.**(c)** Equivalence to plane only visualisation of defect chains.

$$\frac{d\mathbf{p}_i}{dt} = \frac{\partial \mathcal{H}}{\partial \mathbf{x}_i} = -\sum_{j \neq i} \frac{\partial V_{ij}}{\partial \mathbf{x}_i} - \lambda_i \frac{\partial g}{\partial \mathbf{x}_i} \tag{28}$$

$$\mathbf{x}_i^m - \mathbf{x}_i^{m+1} + \Delta t \left(\mathbf{p}_i^m + m_i^{-1} \Delta t \left(\mathbf{f}_i^m - \lambda_i^m \mathbf{n}_i \right) / 2 \right) = 0 \tag{29}$$

$$g(\mathbf{x}_i^{m+1}) = 0 \tag{30}$$

chain originated from the particle i.

Imagine that a two-dimensional lattice is relatively simple to consider, whereas if we assign different curvature properties to lattice points at different locations, i.e., lattice points at a specific number, with their respective positive/negative curvature corresponding to the Hamiltonian quantity, and then consider it as a bond. We erase the external field (consider that this is a surface with only slight undulations) and consider only the interactions between the particles, this would greatly simplify the model as Fig. 15,The Hamiltonian quantity in this system can be expressed as

$$\begin{aligned} H = &-\epsilon_{ij} \sum_{\langle i,j \rangle} \Theta \left(\vec{\sigma}_i \cdot \vec{e}_{ij} - 1 \right) \cdot \Theta \left(\vec{\sigma}_j \cdot \vec{e}_{ji} - 1 \right) \\ &- \epsilon_{ik} \sum_{\langle i,k \rangle} \Theta \left(\vec{\sigma}_i \cdot \vec{e}_{ik} - 1 \right) \cdot \Theta \left(\vec{\sigma}_k \cdot \vec{e}_{ki} - 1 \right) \end{aligned} \tag{31}$$

Among other things, we make the following idealised assumptions:

$$|\vec{\sigma}_i| = 1 \tag{32}$$

$\vec{\sigma}_i$ is the orientational vector of the dislocation

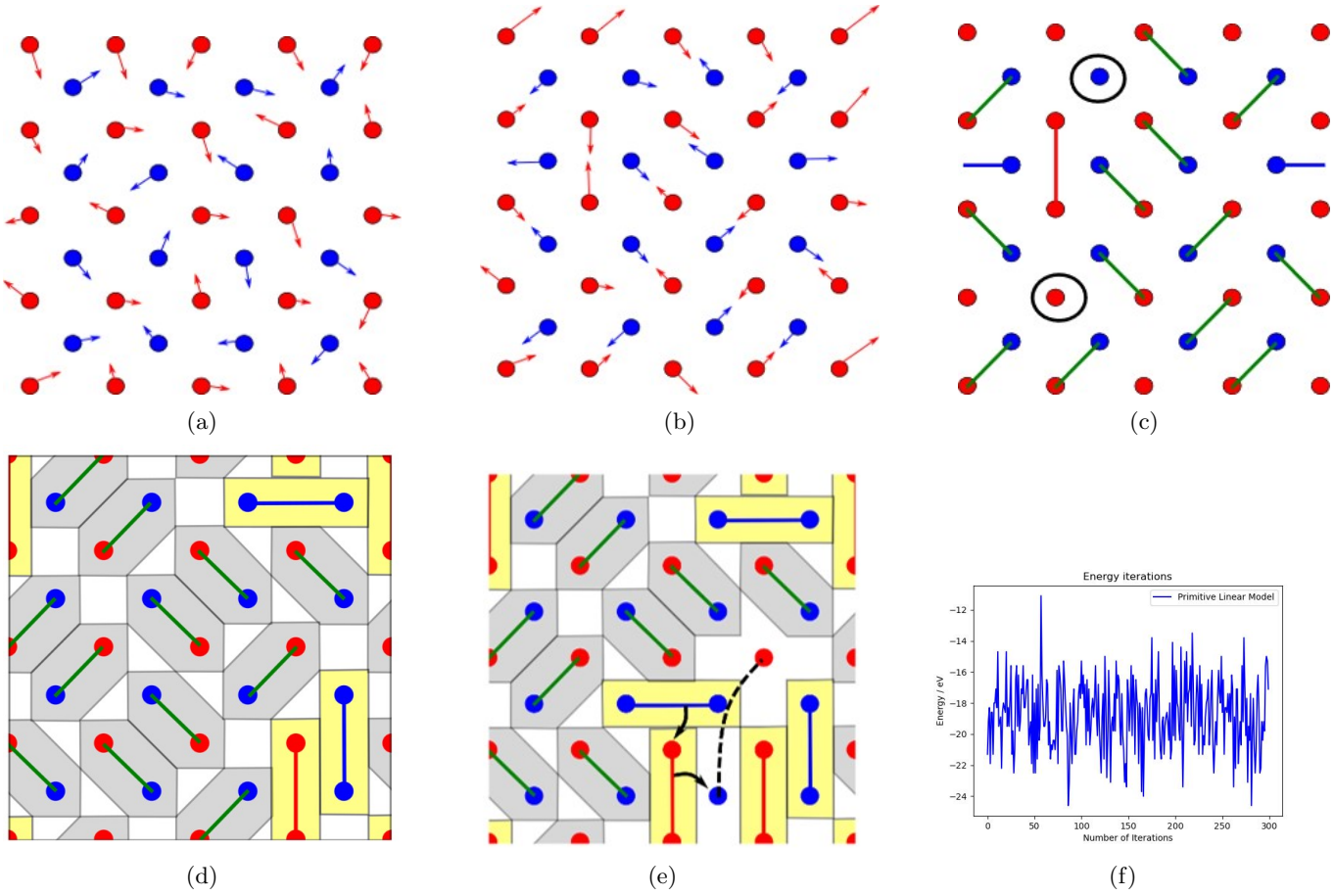

FIG. 16: **Dimer model applied to the interaction patterns of lattice particles on sinusoidal surfaces.** **(a)** shows the energy iteration plot for the linear model, the red line in **(b)** represents the iteration plot for the cosine model, and the blue line represents the iteration plot for the linear model. It can be seen that the cosine model does not converge to a certain point.**(c)**We only consider the nearest neighbour and next nearest neighbour actions, then there are only two cases for lattice points, denoted by green and red lines.**(d)**Simplified square dimer model. The green lines correspond to directional flows on different curvatures, and the red and blue lines represent directional flows on the same curvature.**(e)**indicates the consequences of one of the directional choices. Here the pairing of lattice points between the same curvature results in the failure to pair lattice points between different curvatures, which in turn affects the energy.**(f)**Schematic of energy simulation, which can be seen to fluctuate, but generally stays within limits.

$$\Theta(x) = \begin{cases} 0 & x < 0 \\ 1/2 & x = 0 \\ 1 & x > 0 \end{cases} \tag{33}$$

$\Theta(x)$ is the Heaviside step function.
$\vec{e}_{ij}$ is a unit vector pointing from the particle i to the particle j.

It is worth noting that the model can be more accurate by considering the interaction between full chains. Here, we ignore the higher order term to keep it simple. In summary, we note that neither individual disclinations nor single dislocations can be produced through any kind of continuous transformation since they are topological defects. However, when produced via appropriately formed pairs, they can: dislocations from (5, 7, 5, 7) clusters, and disclinations from (5, 7) dislocations.[19]The simplified dimer model greatly facilitates our computer simulations. As we mentioned earlier, if we encode the different types of topological defects separately (here we encode the defects at positive curvature as "1", the defects at negative curvature as "-1", and the part without topological defects as "0") and consider different combinations of bonding. What we are really interested in is the bonding of two or two different types of particles - this means that the statistical properties of the system change and the total energy of the system changes. Using our knowledge of thermodynamics and statistics, we know that eventually the system will tend to proceed in the direction of increasing entropy - that is, this curved lattice system is most stable when the energy drops to a minimum.

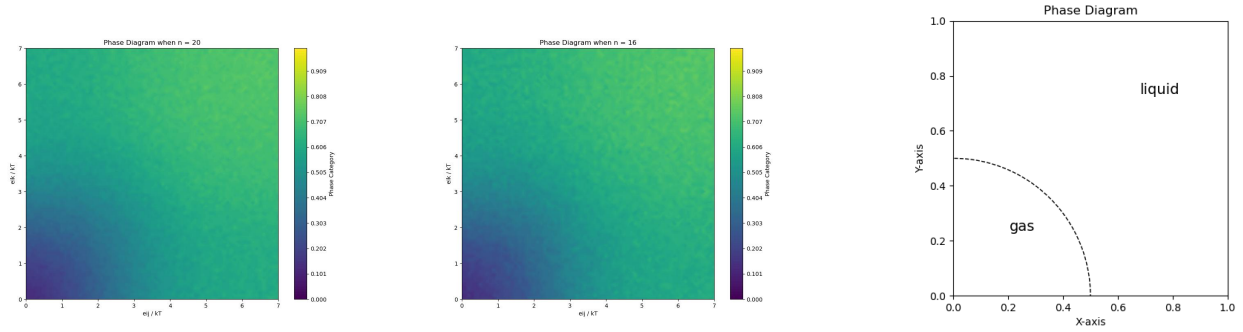

(a) (b) (c)

FIG. 17: **Variation of bonding ratios with different parameters. (a)** shows plot of the change in the proportion of particles bonded when n=20. And **(b)** shows plot of the change in the proportion of particles bonded when n=16.**(c)**Phase diagram plotted from (a) and **(b)** after critical point extraction fitting.

Following this consideration, we use Monte Carlo's method to simulate the motion process of the plane. The system is made to change randomly, the total energy of the new system is calculated for each frame, and the new energy is accepted when it is within a certain range compared to the old energy variable.

The energy range in the real simulation is shown in Fig. 16 We see that the energy stabilises over a certain range, which can be considered to be the steady state energy of the system - the system is in a state of dynamic equilibrium. When ϵ_{ij} ,ϵ_{ik} are fixed, the energy changes are independent of the choice of direction within a certain range.This is consistent with the results in the square dimer model we discussed earlier. The reaction to the physical image is that this system will eventually undergo coalescence, which can be considered as the phase transition we are interested in.

The phase transition variables of the system are related not only to the selection of the model, but also to the parameters of the forces between neighbouring particlesϵ_{ij} ,ϵ_{ik} . By the statistical nature, the bonding number ratio can be used as a parameter for us to examine the morphology of matter. Since the phase transition process here does not belong to the continuous phase transition, we cannot use the theory of reorganisation groups to study it. Therefore, for the simulation of the phase transition, we use the same Monte Carlo method to simulate the properties of the system under different ϵ_{ij} ,ϵ_{ik} conditions by scanning the bonding ratios of the subsystems under different ϵ_{ij} ,ϵ_{ik} correspondences.

If ϵ_{ij} and ϵ_{ik} are fixed, and we then examine how the fraction varies with temperature, this fraction exhibits a behavior similar to the hyperbolic tangent function theoretically.18 The inflection point is around 0.5, where the rate of change is maximal, which can be considered as a boundary. Here, we assume the gas phase when the total bonding ratio is less than 0.5, and the simulation diagrams are shown in Fig. 17.

We note that the number of bonding here is not only

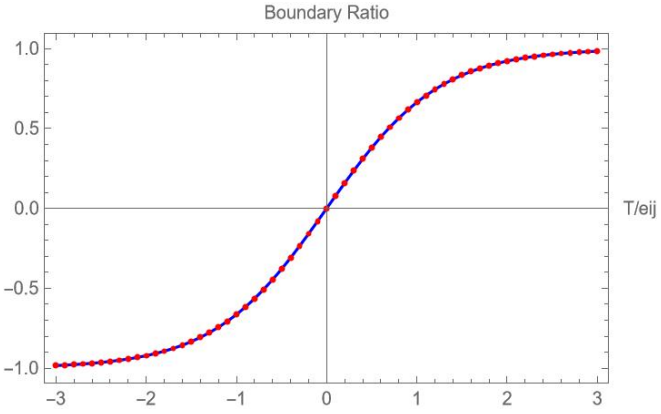

FIG. 18: **Relationship between boundary and temperature in theory.**It shows like hyperbolic tangent function, where we define the point where first order derivative is at its maximum is the boundary point.

related to ϵ_{ij} ,ϵ_{ik} but also to n. Here we ignore other interacting forces and possible low-field conditions and take into account the bonding of both the first and second neighbours. It is interesting to note that whether the variable is ϵ_{ij} or ϵ_{ik}, initially the first neighbour takes up most of the bonding, and as ϵ_{ij} ,ϵ_{ik} is raised, the bonding ratios of the second neighbours only gradually catch up. This is in accordance with the familiar physical picture of the phase transition process.

IV. DISCUSSION

We have modelled the motion of particles on surfaces by means of an approximation of molecular pseudo-dynamics, introducing the dimer model as an illustration of the projection of the lattice onto a two-dimensional plane and a relatively artificial specification of the point

of phase transition formed by the model's spin coupling into bonds. If we extend the upper limit of the modelled data (20 kT and above), we should be able to observe the transition from the liquid to the glassy state,which is a short-range ordered and long-range disordered state. It should be in the state of hexagonal phase in this interval. And this phase transition process is not a first-order phase transition. We are solving this type of model because this model is not a continuous phase transition and there is no way to simplify it using the theory of renormalization groups theory.

Experimentally, it is challenging if we need to simulate such a situation. We need to ensure that the particles are bound to the surface in the external field, and that the interactions between the particles are such that the particles are essentially not displaced by more than the radius R of the particles. It is also debatable that we did not take into account the short-range forces when performing the actual simulations and also did not take the shielding effect into account. However, the idea of computer simulation is still informative for the approximation of the treatment of chain defects on curved surface.

The elucidation of order by the unravelling and flattening of an appropriate polyhedral net may be useful in other contexts, such as liquid crystalline orientations on curved surfaces (for example, the tetrahedrally symmetric, baseball-like texture of a nematic confined to a thin shell, Supplementary Information section 8.6[20]).

V. CONCLUSION

Through the above introduction we have carried out a theoretical analysis of the stable lattice model on surfaces, and modelling and computer simulation of surface lattices.

The Gaussian curvature and inherent topological defects of curved plane will result in pentagons and heptagons in crystal structure which means additional dislocations. They may further influence the stability, mobility, interactions, and dissociation of dislocations, thereby affecting the KTNHY process and leading to more complicated phase transitions. In many cases, linear dislocation arrays, i.e., topological defect chains are formed to reduce elastic strain energy better.

We introduced the Potts model, for the distribution of curvatures of the surfaces we will study subsequently and the formation and distribution of defect chains on it is similar to the $q = 8$ Potts model.We also introduce the dimer model, which describes the topological relationships corresponding to the lattice at different numbers of edges using height functions. We introduce the dimer model to explain the embedded crystal model, introduce the weight functions and physical implications, and apply them to simulations. In our simulations, we simplify the surface to a two-dimensional plane and compare the energies at different Hamiltonian quantities. In practice, there may also be cases of low fields, and other forces. Interested readers can follow this idea for further analyses and simulations. In the phase transition section, we calculate and assume 0.5 bonding ratio for gas-liquid criticality . Although such a consideration ignores many cases (carried out in extremely idealised scenarios), it provides a reference for how we deal with phase transitions in dimer models.

The curved lattice problem will be widely used in bioengineering, medicine and other fields. Transport of drug carriers, crystallisation under special surfaces, etc. will be bridged between traditional physical images by the discussion of surface defect chains. As in our study, the need for both crystalline order parameters and dimer model has been invoked in recent models of assembly of stable distribution of active medicinal ingredients of rule surface. Moreover, the segregation of defects to symmetric sites, and the concomitant mobility near these sites, should prove useful in designing structures where both rigidity and fluidity are desired in specific areas.

ACKNOWLEDGMENTS

We received theoretical guidance and help from Prof. Peng Tan and Postdoctoral Fang Huang during the honours course thesis, and the data references for the surface visualisation came from Postdoctoral Fang Huang, for which we are very grateful.

Appendix A: Monte Carlo Simulation

More details of the simulation and the original code are available at https://github.com/sslownn/statistical-mechanics-paper-chaindefect.git.

Appendix B: Proof for Theorem

Let G be a finite, bipartite, planar directed graph with a weight function defined on its edges. Since G is bipartite, color the vertices black and white and label them as $w_i \in W$, $b_j \in B$, and any (unoriented) edge in G will be labeled by a pair (w_i, b_j). The Kastelyn matrix associated to G is the following oriented weighted adjacency matrix:

$$K_{ij} = \begin{cases} v(\mathrm{w}_i b_j), & \text{if } w_i \to b_j \\ -v(\mathrm{w}_i b_j), & \text{if } b_j \to w_{i'} \\ 0, & \text{else.} \end{cases}$$

WLOG, suppose G has $2n$ vertices, with n of these vertices white and n black. If this is not the case, there will be no dimer configurations on G. Consider the determinant of K:

$$\det(K) = \sum_{\sigma \in S_{2n}} \mathrm{Sign}(\sigma) K_{1\sigma(1)} K_{2\sigma(2)} \dots K_{n\sigma(n)}.$$

By inspection, each nonzero term in the determinant corresponds to the Boltzmann weight of a dimer configuration, up to an overall sign. Furthermore, it is also clear that for every distinct dimer configuration M on G there exists a unique nonzero term in the determinant.

Thus, if we can prove the existence of an admissible orientation on the edges of G such that the signs of all terms in the determinant are the same, the proof will be completed. This is not extremely difficult, but it is fairly involved and not the most enjoyable proof to work through. The treatment of this point there is understandable and explicit.[6]

Appendix C: Division of labour details and marking weights

Chen Qi and Chen Yuan together carried out the study and each completed half of the essay.

Chen Yuan undertook the first half of the paper on the description of the geometric defects, the description of the KTNHY theory the potts model and half of the conclusion.

Chen Qi did the simulation and got the data, and completed the parts of dimer model description, simulation interpretations, the abstract, the introduction ,discussion, appendix A and B and half of the conclusion.

After group discussion Chen Qi assigned a score of 66.7 and Chen Yuan assigned a score of 33.3.1

[1] Nelson, D. R., & Halperin, B. I. (1979). Dislocation-mediated melting in two dimensions. Physical Review B, 19(5), 2457.

[2] H.H. von Gr unberg, P. Keim, G. Maret.(2007).Phase Transitions in Two-Dimensional Colloidal Systems,7-11.

[3] Bausch,A. R. et al.(2003) Grain Boundary Scars and Spherical Crystallography. Science,299, 1717.

[4] Rodrigo,E. G. et al.(2018) Freezing on a sphere. Nature,554, 346-348.

[5] Wu F.Y.(1982) The Potts model. Reviews of Modern Physics,54(1), 235-268.

[6] Mike Gartner, (2014),Classical and Quantum Dimer Models.ArXiv:2309.14447

[7] Timothy Fong Nam Chan(2016),Dimer Models and Their Characteristic Polygons.

[8] Fowler, R H. and Rushbrobke, G. S., Trans. Faraday Soc. 33 (1937) 1272.

[9] Muir, T., Contributions to the History of Determinants, London (1930). Scott, R. F. and Mathews, G. B., Theory of Determinants, Cambridge University Press, New York (1904) 93.

[10] Hurst, C. A. and Green, H. S., J. chern. Phys. 33 (1960) 1059.

[11] P. W. KasteleynThe Statistics of Dimers on a Lattice-Physica.27(1961) 1209-1225.

[12] R. Kenyon, A. Okounkov and S. She eld, Dimers and Amoebae, math-ph/0311005.

[13] B. Tiliere, The Dimer Model in Statistical Mechanics.

[14] Witten, E. (2001). String theory in various dimensions. Reviews of Modern Physics, 73(3), 121.

[15] Feynman, R. P., & Hibbs, A. R. (1954). Quantum Mechanics and Path Integrals. New York: McGraw-Hill.

[16] Einstein, A., Podolsky, B., & Rosen, N. (1935). Can quantum-mechanical description of physical reality be considered complete?. Physical Review, 47(10), 777.

[17] Lamport, L. (1994). LaTeX: A Document Preparation System, 2nd Edition. Addison-Wesley.

[18] H.H. von Gr unberg, P. Keim, G. Maret.(2007).Phase Transitions in Two-Dimensional Colloidal Systems,8.

[19] H.H. von Gr unberg, P. Keim, G. Maret.(2007).Phase Transitions in Two-Dimensional Colloidal Systems,11.

[20] Vitelli, V. Nelson, D. R. Nematic textures in spherical shells. Phys. Rev. E 74, 021711 (2006).